



Fractal geometry and multifractals in analyzing and processing medical data and images

Irimi S. RELJIN¹
Branimir D. RELJIN²

A traditional way for describing objects, based on the well-known Euclidean geometry, is not capable to describe different natural objects and phenomena such as clouds, relief shapes, trends in economy, etc. On the contrary, fractal geometry and its extension - multifractals - are new "tools" which can be used for describing, modeling, analyzing and processing different complex shapes and signals. This paper considers fractal geometry and multifractals and their application in signal analyzing and processing, particularly in medical signal analysis.

¹PTT COLLEGE, BELGRADE, YUGOSLAVIA

²FACULTY OF ELECTRICAL ENGINEERING, UNIVERSITY OF BELGRADE, YUGOSLAVIA

KEY WORDS: *Fractals; Fractal Dimension; Multifractals; Signal and Image Processing*
Archive of Oncology 2002,10(4):283-293©2002,Institute of Oncology Sremska Kamenica, Yugoslavia

INTRODUCTION

Traditionally, objects and phenomena are described by using different measurements, called *dimensions*. (The word dimension is derived from the Latin word *dimensio*, which means measure.) For instance, let us assume that we want to completely characterize some ordinary object as, for instance, a tree. To achieve that, we have to measure its height, width, length, number of branches and subbranches, color, density, etc. We need a number of different descriptors if we intend to characterize an object as well as possible. The most familiar dimension is the Euclidean one, D_E , known and used since more than 2,300 years ago. The second one is known as the topological dimension, D_T . They both can assume only the integer values 0, 1, 2, 3, and in most cases they are used as synonymous since for many objects they can be the same (1). But some differences exist as we will describe in short. (Truth to say, many authors do not distinguish the topological and the Euclidean dimension.)

The topological dimension is defined regarding the way how an observed object can be divided, while the Euclidean one considers the space occupied by an object. For instance, the point is dimensionless, since the point is not a continuum and, thus, both

Euclidean and topological dimensions are the same, $D_E=D_T=0$. Regarding the line and other figures the differences between these dimensions arise. From the topological point of view the line has the dimension $D_T=1$, irrespective of the shape of the line, since it can be divided by points that are not continua. Similarly, to divide surfaces, curves are necessary. So, the topological dimension of surface is $D_T=2$, and, in a similar way, the topological dimension of a space is $D_T=3$, since to divide space, surfaces are necessary. According to the Euclidean definition, a structure is called one dimensional (1D) if it is embedded on a straight-line, two dimensional (2D) if it is embedded on a plane, and three dimensional (3D) if it is embedded in space. From this definition only the straight line is one dimensional, $D_E=1$, since it does not occupy either the plane or the space. But, the curve line lying in the plane has the dimension $D_E=2$ while the complex curve lying in the space is three dimensional, $D_E=3$. Also, the flat surface is two dimensional, $D_E=2$, but non-flat surface can be assumed as three dimensional, see Figure 1.

Artificial objects are characterized by smoothness and structural regularity. The description of such objects is quite easy by using an adequate dimension. The object dimension can be measured and numerically described by comparing it with some referent sample measure unit. For instance, the weight can be derived comparing it with the reference weight of 1 kg, the length - by comparing it with 1 m, etc. But, also, the curve length can be derived analytically, through the line integral, the surface area can be derived from the surface integral, the volume and/or the object weight can be derived from an appropriate volume integral, etc. Certainly, the use of integrals assumes that the corresponding

Address correspondence to:

Irimi Reljin, PTT College, Zdravka Čelara 16, 11000 Belgrade, Yugoslavia, E-mail: iririnir@telekom.yu

The manuscript was received: 17. 06. 2002.

Provisionally accepted: 05. 07. 2002.

Accepted for publication: 09. 07. 2002.

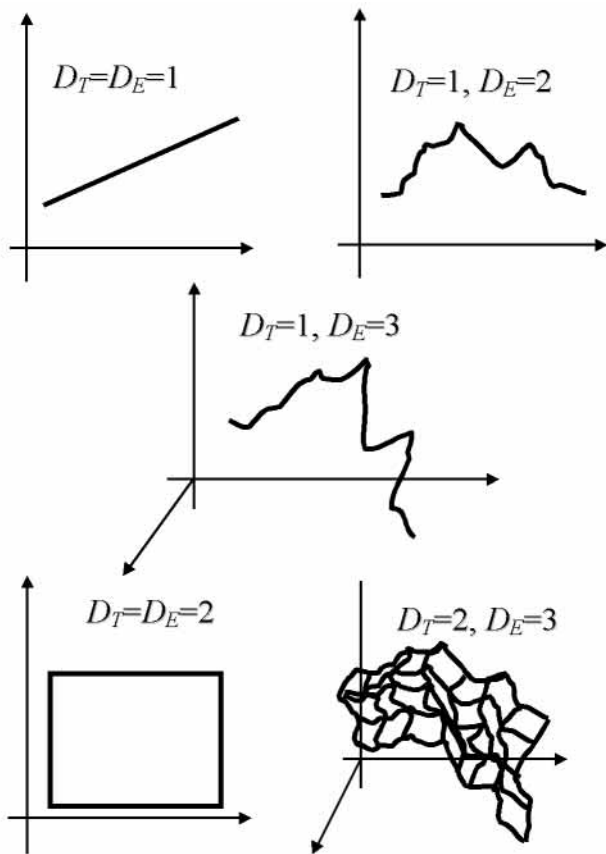


Figure 1. Examples describing differences between topological and Euclidean dimension

function is differentiable. The Euclidean geometry was the basic concept used in designing, constructing and describing all artificial objects during many centuries.

Today, measuring of length, area and volume appears to be no problem. As an illustrative example consider a classic smooth object as, for instance, a telephone wire of the length of 1,823.25 m. Then, by using different measure units we will obtain only different precision of measured length; particularly, if the unit is 100 m, the length of "more than 1,800m = 18x100m" will be obtained; if the unit is 10m, the length of "more than 1,820m=182x10m" will be reached, etc. By using smaller and smaller measure units more precise length is obtained, converging to the finite value.

But, what is with irregular shaped objects such as a coast line? The famous Mandelbrot's paper printed in 1967, "How long is the coast of Britain? Statistical self-similarity and fractional dimension" (1), demonstrated that the classic way of measuring the length is useless in this case - the measured length strongly depends on the measure unit applied¹. The smaller the measure units the longer the resulting measurement will be. Conversely, a regularly shaped object such as, for instance, a circle of diameter d , has finite perimeter P . Depending on the measure unit used only the accuracy of the measured perimeter varies, but the

length converges to the limiting value of $P=\pi d$.

The coastline exhibits classic *self-similar* (or, fractal) behavior. By observing the structure of the coastline in different scales (almost) the same shape arises. Analytically speaking, the coastline is not differentiable in all points and, thus, the line integral is not defined. The difference between fractal and smooth line is illustrated in Figure 2.

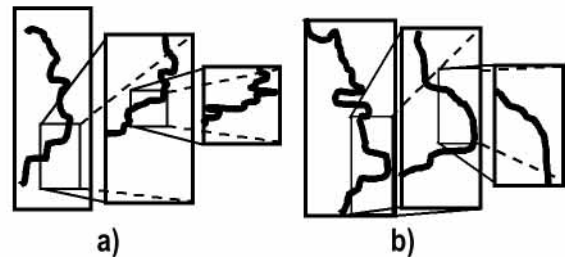


Figure 2. Difference between (a) fractal and (b) smooth line

The word *fractal*, introduced by Mandelbrot, the Polish born mathematicien, is derived from the Latin adjective *fractus* (broken). This term was used to describe the irregular structure of many natural objects and phenomena. Simple fractal rules can often describe these structures in a way that conventional techniques cannot (1-3).

The central philosophical theme of fractal geometry is that nature - despite its complexity - exhibits a fundamental property generally known as *self-similarity* (2). That means, however a complex the shape and/or dynamic behavior of a system, by observing it carefully and imaginatively enough, one can find features in one scale which resemble those at other scales. Remeber the structure of the tree, for instance. If we break a branch from the tree, its shape has similar structure but to a smaller scale. By breaking a twig from the branch the structure repeats, etc. A similar structural behavior can be found by observing a cloud, some vegetables (cauliflower, broccoli), venous and arterial system, nervous system, the Earth relief, trends in economy, etc. Also, self-similar structures can be generated artificially, by using some predetermined rules. This kind of self-similarity has found significant place in modern art, but also in science and technique. As an illustrative example, in Figure 3 the fractal coast - as a remarkable example of self-similar structure - is depicted. Starting from the upper left image, by magnifying its central part (within the white rectangle), after six iterations exactly the same initial structure is obtained. That means, this structure is self-similar of infinite complexity (1).

The self-similarity is clearly not a new concept and most of us have at some stage thought in this way. The origin of this aspect of mathematics is associated with a number of specialists dating from the middle of the nineteenth century², but the systematic approach and, consequently, the completely new concept of

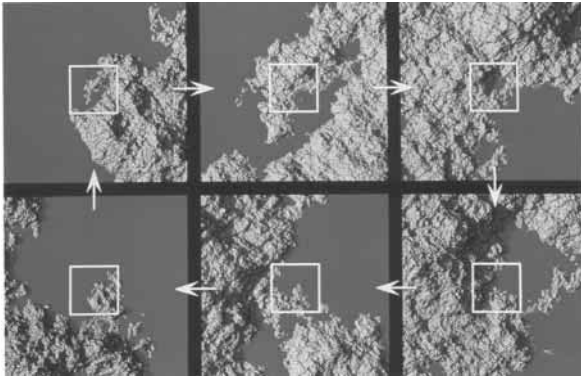


Figure 3. Self-similar object - fractal coast - of infinite complexity: repeating after 6 magnifications, (c) R.F. Voss, from (1)

geometry, is introduced by Mandelbrot. Having in mind Cantor's words "The art of asking the right questions in mathematics is more important than the art of solving them", it is not surprising why Benoit Mandelbrot is characterized as the "father of fractal geometry" (1).

Artificially generated fractals, by applying precise algorithms and rules, exhibit hard fractal behavior, as we will describe in next section. Conversely, natural objects and phenomena, do not exhibit so strict fractal behavior even when they are classified as fractals (for instance, the cauliflower). Natural objects have statistical self-similarity: by observing their structure in different scales the similar but not exactly the same structure is obtained. In this case we will consider *multifractals* rather than fractals. Multifractal parameters, used for describing such structures, can be applied in the object classification (4), enabling a new approach in investigation many phenomena, besides others in medical diagnosis.

The paper is organized as follows. In next two sections a brief review of fractals and multifractals is exposed. In the last section the application of fractals and multifractals in medical signal analysis, particularly in medical image analysis, is explained, in brief.

DESCRIPTIONS OF FRACTAL GEOMETRY

A. Fractal objects and signals

Measuring, describing and comparing different objects is usually made by using some dimensions, as we noted earlier. But, how to measure fractals? Recall that a point is dimensionless, its Euclidean dimension being $D_E=0$. But, observe a series of adjacent points, as in Figure 4. If the distance d between adjacent points is small enough, the obtained structure is line-like. What is the dimension of this structure? When the distance approaches to zero, $d \rightarrow 0$, the continuous line will be obtained, having the dimension of 1. So, the discrete structure depicted in the middle of Figure 4 has the non-integer dimension (fractal dimension) between the limiting values 0 and 1. Such a structure is known as

a *fractal dust*. Furthermore, a flat sheet of paper has the Euclidean dimension $D_E=2$. If we scrunch up it into a ball, the obtained structure is a volume, having the dimension $D_E=3$. But, when we unfold a paper, the new structure is neither a sheet nor a ball. This structure occupies the space but not completely. What is the dimension of this structure? Somewhere between 2 and 3! These surprising conclusions belong to the concept of the *fractal dimension*, permitting the description and comparison of different com-

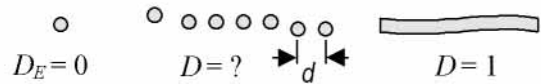


Figure 4. Illustration of the concept of fractal dimension

plex shapes and phenomena.

Fractal shapes and signals are characterized by the following features (1-2):

- 1. They do not have characteristic (finite) length.** This feature is documented over the coast line example. The smaller the setting of the measuring device, the longer the resulting measurement will be, since the more details are accounted. On the contrary, smooth curve has a definite length and it can be measured as accurately as necessary.
- 2. They exhibit the self-similarity behavior.** A structure is said to be self-similar if it can be broken down into arbitrary small pieces, each of which is a small replica of the entire structure. Small pieces can be obtained from the entire structure by a similarity transformation - by using a scale factor less than unity. For instance, as producing copies from the photocopier machine. However, note that if a structure is self-similar it needs not to be fractal.
- 3. They have non-integer dimension,** usually greater than corresponding Euclidean dimension.

B. Deterministic fractals

Deterministic fractals are artificially generated structures obtained under a simple production rule. There is no element of randomness in the object production. The generation of deterministic fractal starts with the initial element - the *initiator*, which is scaled down with the scale factor, $r < 1$, and modified by applying the *generator* or the *production rule*. Several examples of deterministic fractals will be reviewed here.

B.1. Cantor Set The initiator is a line of length d . The production rule is as follows: Divide a line by 3; remove its middle third; repeat the procedure for each of two remaining parts. Continue on in this way. In each step the same structure is obtained but to a



Figure 5. Cantor Set: the initiator (the first row) and the first four construction steps

smaller scale (1). Figure 5 visualizes the construction from the initiator (the first row) to the fourth step.

B.2. Von Koch Curve The initiator is a line of length d . The production rule is: Take the initiator; divide it by 3; replace its middle third by two equal segments of side $d/3$ forming an equilateral triangle; repeat the procedure for each of four lines of length $d/3$. The procedure is illustrated in Figure 6, for the first three suc-

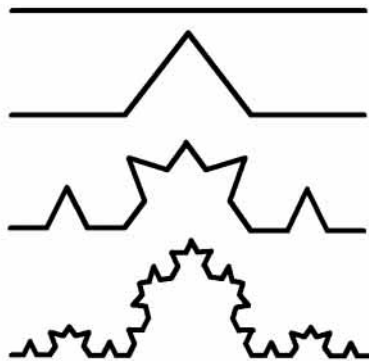


Figure 6. The first three steps in the construction of the Koch Curve

cessive steps (1). A version of the Koch Curve is the *Koch Snowflake* (or, *Koch Island*). The initiator is a polygon, for instance an equilateral triangle as in upper left side in Figure 7. The production rule is the same as for the Koch Curve, as depicted in Figure 7 for the first three steps.

Note that the Koch Curve and the Koch Snowflake tend to have infinite lengths after infinite iteration steps. Namely, assuming the initiator has the length of unity, $d=1$, after the first step the obtained structure has the length $d_1=Nxr=4 \times 1/3=4/3$, since the number of copies is $N=4$, and the scale factor is $r=1/3$. After the second step the length is $d_2=N \times (Nxr) \times r=(Nxr)^2=(4/3)^2$, i.e., after the i th step the length is $d_i=(Nxr)^i=(4/3)^i$. The Koch Curve (Snowflake) is continuous but nowhere differentiable as $i \rightarrow \infty$. Note that the Koch Snowflake always has a finite area. The

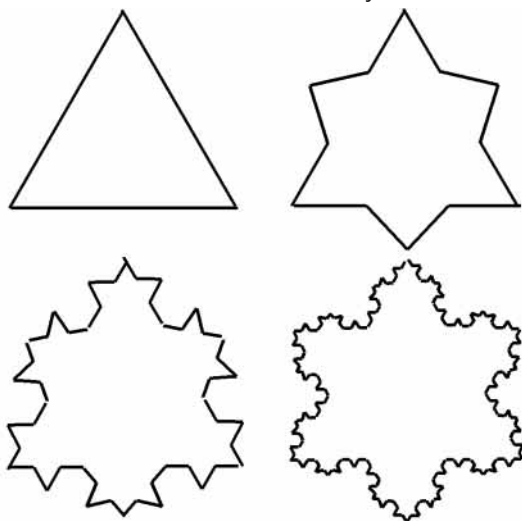


Figure 7. The initiator and the first three steps in the construction of the Koch Snowflake

unforeseen property that the curve has infinite length but finite area is one of the reasons why such curves are known as the "monster curves".

B.3. Sierpinski Carpet The initiator is a rectangle, upper left in Figure 8. The production rule is: Take the initiator; divide each side by 3; remove the middle part; repeat the procedure for each

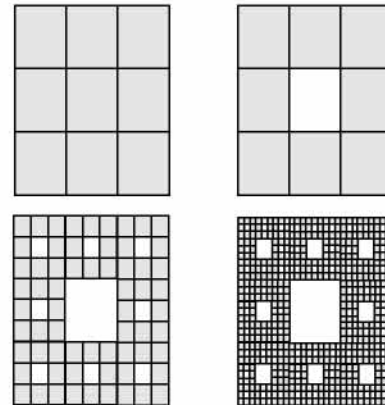


Figure 8. The initiator and the first three steps in the construction of the Sierpinski Carpet

of eight remaining parts.

C. Characterization of fractal structures

A fractal dimension is a fundamental analytical parameter for describing self-similar structures. Traditionally, monster curves or surfaces are classified via point-set topology. Remember that curves have a topological dimension of one, surfaces have a dimension of two, etc. Historically, Felix Hausdorff was the first who defined a non-integer dimension in describing monster functions (5). It is not trivial to calculate the *Hausdorff* (or *Hausdorff-Besicovitch*) dimension for even simple sets (1-2). Later on, several methods for determining fractal dimension were derived (1-3). For deterministic fractals fractal dimension is assumed as a *similarity dimension*, D_s .

For a bounded set A in Euclidean n -space is said to be self-similar if A is the union of N non-overlapping copies of itself, each of which has been scaled down by a ratio $r < 1$ in all coordinates. Between N and r the following relation is valid

$$Nr^{D_s} = 1 \tag{1a}$$

wherefrom the similarity dimension is

$$D_s = -\frac{\ln N}{\ln r} \tag{1b}$$

From (1) the similarity dimension for the Cantor Set is

$$D_s = -\frac{\ln(2)}{\ln(1/3)} \cong 0.631$$

since this structure is generated from $N=2$ parts (lines) repeated into the scale $r=1/3$. Instead of initial line (having dimension

$D_E=1$), the structures in next steps tend to line-like quasi-point form having fractal (similarity) dimension between zero and unity. For the Koch Curve, generated by the procedure illustrated in Figure 6, the similarity dimension is

$$D_s = -\frac{\ln(4)}{\ln(1/3)} \cong 1.262$$

since $N=4$ and $r=1/3$. Instead of the straight-line (initiator), having $D_E=1$, the successive structures partially occupy a space, so, the dimension is greater than unity. Similarly, for the Sierpinski Carpet the similarity dimension is

$$D_s = -\frac{\ln(8)}{\ln(1/3)} \cong 1.893$$

The ranges in the value of fractal (similarity) dimension characterize the type of the fractal. The structure having the fractal dimension between 0 and 1 is known as the *fractal dust*, the structure having the fractal dimension between 1 and 2 is the *fractal signal (fractal line)*, the structure with dimension between 2 and 3 is the *fractal surface (fractal image)*, while the structure with dimension between 3 and 4 is the *fractal volume*.

For better distinguishing fractals and non-fractals let us observe the objects as in Figure 9: the straight-line and the rectangle. Both objects (also the cube, not shown) are self-similar: each can be broken into small copies, which are obtained by similarity transformations. For instance, if the line (Euclidean dimension $D_E=1$) is divided by 3, i.e., of the scale factor $r=1/3$, one obtained $N=3$ parts. The fractal dimension of the obtained structure is

$$D_s = -\frac{\ln 3}{\ln(1/3)} = 1$$

which is identical to the Euclidean dimension of the straight-line. The structure is self-similar but it is not fractal. A similar conclusion can be derived for the rectangle (Euclidean dimension $D_E=2$) in Figure 9. By scaling each side with the scale factor $r=1/3$, we obtain $N=9$ parts, each of them as a copy of initial figure. The fractal dimension of the new structure, from (1), is equal to the Euclidean dimension

$$D_s = -\frac{\ln 9}{\ln(1/3)} = 2$$

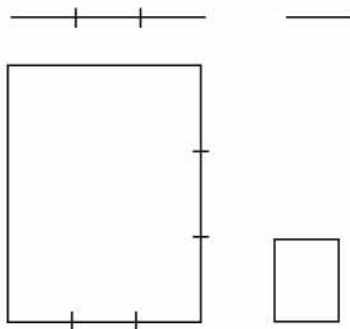


Figure 9. Self-similarity of a line and a square

The structures in Figure 9 are self-similar but they are not fractals: after scaling, the complexity of structures remains unchanged. The general conclusion can be derived: fractal objects exhibit the self-similar behavior but the opposite conclusion needs not be fulfilled.

Natural fractals have not so regular structure as deterministic fractals. For instance, a magnified section of a coastline will resemble the whole in some way but not exactly. This structure exhibits *statistical self-similarity*. For such structures the similarity dimension, given by Equation (1), is not appropriate, since no precise production rule. Different methods for determining the fractal dimension of such structures are derived. One of the most popular algorithms for computing the fractal dimension is the *box-counting method*, or the *covering method*. The method involves covering a fractal with a grid of n -dimensional boxes (hyper-cubes) with a side length ε and counting the number of non-empty boxes, $N(\varepsilon)$. For 1D signals (as time series) the grid is one of squares and for 2D signals (as images), a grid of cubes. Then the log-log plot of $N(\varepsilon)$ and $1/\varepsilon$ is made. Now change a side length progressively to smaller sizes and count the corresponding number of nonempty boxes. From the slope of the fitted straight-line to the plotted points of the diagram we derive the box-counting dimension D_B . Namely, as a limiting value, when $\varepsilon \rightarrow 0$ the number of boxes is proportional to ε^{-D_B} , i.e.,

$$D_B = -\lim_{\varepsilon \rightarrow 0} \frac{\log N(\varepsilon)}{\log \varepsilon} \quad (2)$$

Note that for a large scale of fractals, including classic fractals such as the Cantor Set, the Koch Curve, the Sierpinski Carpet, etc., the Hausdorff dimension and the box counting dimension are very close, but this needs not to be fulfilled in general (6).

Figure 10 illustrates the procedure of box-counting method. The 1D signal over the length $L=1$ (time, for instance) is under observation. If the box size is $\varepsilon_1=1/10$, Figure 10a, the number of non-empty boxes is $N_1=25$, and the corresponding box-dimension is $D_{B1}(\varepsilon)=1.398$, obtained from $\log(25)/\log(10)$. With smaller boxes, for instance $\varepsilon_2=1/20$, Figure 10b, the number of non-empty boxes is 38, thus $D_{B2}(\varepsilon)=1.214$, as $\log(38)/\log(20)$. In limiting case D_B will approach the final value corresponding to Equation (2).

Except the fractal dimension (the Hausdorff-Besicovitch dimension, the similarity dimension, the box-counting dimension), the fractal (self-similar) object can be described alternatively by some other descriptors, for instance, by *compass dimension*, the *Hurst index (H)*, etc. (1). The compass dimension is very useful in determining line-like fractals (as a coastline). The Hurst index was introduced by H. E. Hurst, a British hydrologist, who investigated the Nile river fluctuations over decades. He established a new

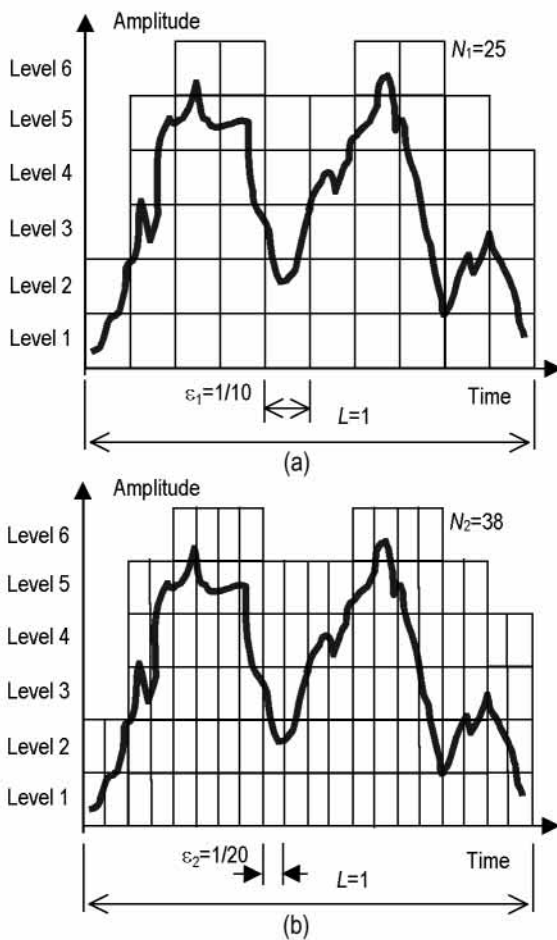


Figure 10. The box-counting method: (a) box size is $\epsilon_1=1/10$, (b) box size is $\epsilon_2=1/20$

nonlinear statistics of scaled ranges known also as the R/S statistics. The H -index can be derived in several ways: through R/S statistics, from the periodogram, index of dispersion, etc. It is possible to establish the relation between the fractal dimension of a random fractal line and the Hurst index

$$D = 2 - H \tag{3}$$

Generally speaking, the process having $H=0.5$ corresponds to a pure Brownian motion (*random walk*) - without any correlations between successive movements of particles. If $H>0.5$ there is a positive correlation between incremental movements: if the graph of movement increases for some $t=t_0, x(t_0)$, then it tends to continue to increase for $t>t_0$ - exhibits the self-similar behavior (known as a *long-range dependency*, too) - and this tendency is as strong as the Hurst index is closer to unity. For $H<0.5$ the opposite is true. There is a negative correlation between the increments (a *short-range dependency*) and the system tends to oscillate.

MULTIFRACTAL SIGNALS AND PHENOMENA

In real world most phenomena cannot be expressed in terms of two limiting states such as: black and white, true and false, hot and cold, 1 and 0, etc. Therefore, these aspects demand more general mathematical objects for a successful description of levels between two limiting states. Those more general objects are called *measures* (1). Instead of one quantity, or measure, μ , describing the phenomenon in all scales - when we talk about fractals, a set of measures, $\sum \mu_i$ (a sort of weight factors) describing *statistically the same* phenomenon in different scales has to be used for describing such structures. Consequently, a theory of self-similarity is extended from fractals to multifractals. For instance, consider a 2D signal such as the gray scale image. For describing an object of the image, the box-counting method is not appropriate since it gives only a relation between non-empty boxes and the box size, regardless of the signal level into the boxes. Figuratively speaking, simple counting the boxes is like counting money without caring about the value of banknotes. By considering multifractals the signal value (the measure μ_i) within the box is embedded into the process of signal characterization. At the first step, the quantity α

$$\alpha = \frac{\log \mu(\text{box})}{\log \epsilon} \tag{4}$$

called the coarse *Hölder exponent* (1), is derived. This is the logarithm of the measure of the box, $\mu(\text{box})$, divided by the logarithm of the size of the box. In this way the coarse Hölder exponent corresponds to the fractal dimension of the measure. For a large class of multifractals the value of α is restricted to an interval $[\alpha_{\min}, \alpha_{\max}]$, where $0 < \alpha_{\min} < \alpha_{\max} < \infty$. Note that the value of α is close to the corresponding fractal dimension of the structure under observation; that means that for 1D signals (having the level μ) this value is close to 1, for 2D signals close to 2, etc. Once α has been derived, the frequency distribution of this parameter has to be established, as follows. For each value of α , one evaluates the $N_\epsilon(\alpha)$ of boxes of size ϵ having the coarse *Hölder exponent* equal to α . Since the total number of boxes of size ϵ is proportional to ϵ^{-D_E} , where D_E is the Euclidean dimension of the box, the probability of hitting the value of α is $p_\epsilon(\alpha) = N_\epsilon(\alpha) / \epsilon^{-D_E}$. Drawing the distribution of this probability would not be useful since as $\epsilon \rightarrow 0$ this distribution no longer tends to a limit. Instead, it is more appropriate to consider the functions

$$f_\epsilon(\alpha) = - \frac{\log N_\epsilon(\alpha)}{\log \epsilon} \tag{5}$$

or

$$C_\epsilon(\alpha) = - \frac{\log p_\epsilon(\alpha)}{\log \epsilon} \tag{6}$$

As $\varepsilon \rightarrow 0$, both functions tend to well-defined limits $f(\alpha)$ and $C(\alpha)$ (1). The function $f(\alpha)$ is more widely used. When $f(\alpha)$ exists one has

$$C_\varepsilon(\alpha) = f(\varepsilon) - D_\varepsilon \quad (7)$$

Such definition of $f(\alpha)$ means that, for each α , the number of boxes increases for decreasing ε as $N_\varepsilon(\alpha) \sim \varepsilon^{-f(\alpha)}$. Exponent $f(\alpha)$ is a continuous function of α . In many cases the graph of $f(\alpha)$ has the parabolic shape, having the maximum near $\alpha=1$ (for 1D signals), or near $\alpha=2$ (for 2D signals). The values of $f(\alpha)$ could be interpreted as a fractal dimension of the subset of boxes of size ε having coarse Hölder exponent α as $\varepsilon \rightarrow 0$. Namely, when ε tends to 0, there is an increasing multitude of subsets, each characterized by its own α and a fractal dimension $f(\alpha)$. This is one of several reasons for the term multifractals (1).

The concept of multifractals can be illustrated from the same 1D signal as in Figure 10. The amplitude levels can be assumed as measures - our example has 6 different levels (measures). Table 1 compares the number of boxes covering particular signal level, for two box sizes.

Table 1. The number of boxes covering particular level of the signal in Figure 1., for two box sizes

Level	$\varepsilon_1=1/10$	$\varepsilon_2=1/20$
1	2	3
2	5	8
3	6	8
4	4	7
5	6	9
6	2	3

Several methods for deriving the function $f(\alpha)$, usually called *multifractal spectrum*, are known (1,7-9). The classification of spectra $f(\alpha)$, used in multifractal image analysis, was derived by Levy Vehel (10). The value α gives the LOCAL information of the point regularity: for fixed measure (gray level) each image pixel is characterized by its own value of α . For instance, image points having $\alpha \approx 2$ are points where the measure is regular, i.e., where the probability of the signal changes is small. Points with $\alpha \neq 2$ denote the regions where "something happens" - that means, the non-regular zones exist. For instance, points with $\alpha \ll 2$ or $\alpha \gg 2$ denote regions characterized by a high gradient or the regions of discontinuities of the signal or its derivative, respectively.

The value of $f(\alpha)$ gives the GLOBAL information of the signal. For instance, points on the smooth contour belong to the point-set with $f(\alpha)$ close to 1, since this value corresponds to the Euclidean dimension of the line, while the points on the homogeneous region (surface) have $f(\alpha) \approx 2$, etc. The image analysis, from the fractal point of view, was performed in (11-12). The paper (10) described also an interesting way of applying (an inverse) multifractal analysis in the classification of the microscopic sample images. A similar analysis and object classification from the multifractal parameters was performed later on in (13-14).

MEDICAL SIGNAL ANALYSIS USING FRACTALS AND MULTIFRACTALS

Several papers investigated biochemical and medical signals and shapes, from the fractal geometry point of view (11,15-19). It was shown that, for humans, the fractal dimension decreases after the stress and/or the trauma. For instance, in (20) the fractal dimension of the morphology of the brain cells (the Purkinje cells in cerebral cortex and the pyramidal cells in hippocampus - regions of CAI) after bleeding (the cerebral hypoxia) was under investigation. It was found that for laboratory animals (the pigs) the fractal dimension decreases from the value of 1.72 (Purkinje) and 1.54 (CAI), obtained for the control group, to the values of 1.57 and 1.46 (after medium bleeding of 20%), and to 1.38 and 1.36 (after the hard bleeding of 40%). Similar results were obtained for humans: from the values of 1.62 and 1.54 (Purkinje and CAI), for the control group, to the values of 1.56 and 1.47 (medium bleeding), and to 1.41 and 1.36 (severe bleeding). Similar investigations were performed in (21), by analyzing the heart-rate variability (HRV), measured on the kids after the burn trauma. The R/S diagram of HRV signals is depicted in Fig. 11. As indicated in Fig. 11, the Hurst index decreases as time after the trauma increases: from 0.8 (healthy kids) to 0.7 (two days after the trauma) and even to 0.55 (8 days after the trauma).

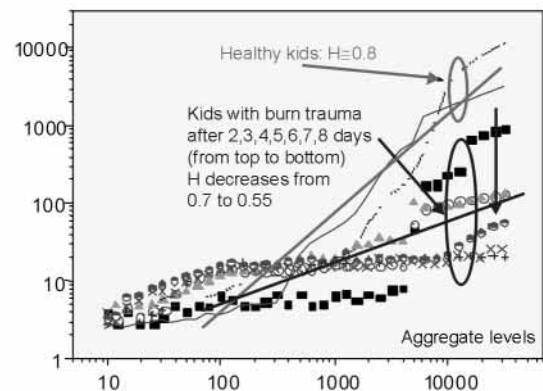


Figure 11. The R/S diagram of the HRV for kids after the burn trauma. The slope of fitted straight-line equals to the H-index

The multifractal analysis (MFA) can be successfully applied in image analysis and object classification. A series of examples in Figures 12-15 illustrates the MFA in object classification. The 256 levels gray-scale medical images of dimension 256x256 pixels were under investigation. Several images were analyzed as 1D vectors (corresponding to scanned images) and the others as 2D signals. As a MFA tool the computer program FALFA embedded into the packet MATPACK (8,9), based on the method derived by Chhabra and Jensen (7), as well as a program HISTMF derived in (13), which is based on the histogram method (1).

Images in Figure 12a-b correspond to digitized microscopy images obtained in the Institute for Pathology and Forensic Medicine at the Military Medical Academy in Belgrade. At first glance, the image in Figure 12b labeled as "Sample 2" resembles to the zoomed version of "Sample 1". However, through the MFA, the difference between these samples is detected. Spectra $f(\alpha)$ of these images are depicted in Figure 12c. The Sample 2 has the broader spectrum $f(\alpha)$, indicating to the higher variability of the signal, while more significant difference is that the maximum of this spectrum is obtained at somewhat greater value of α ($\alpha \approx 1.07$) corresponding to the maximum of the Sample 1 (at $\alpha \approx 1.02$). These differences suggest that the samples belong to different tissues. Note that signals were assumed as 1D and the program FALFA was used.

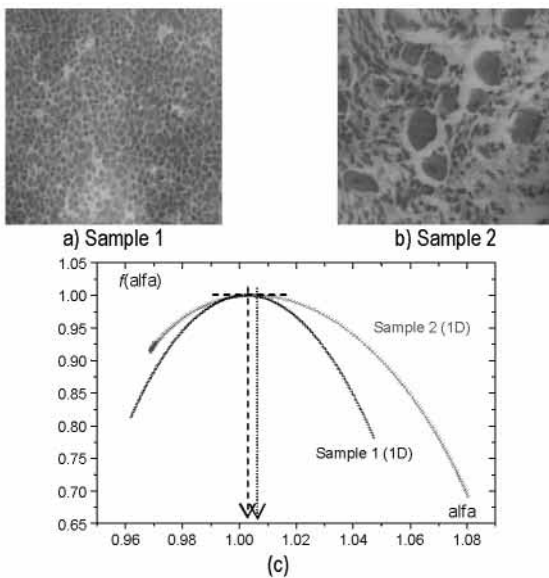


Figure 12. The MFA in sample classification - different samples

The previous results are checked, by using the program HISTMF derived in (13). The results are depicted in Figure 13. Three samples were under the investigation (the first two are the same as in Figure 12). All three samples have different multifractal spectra. Note that the program HISTMF uses 2D signals, thus the $f(\alpha)$ has the maximum near to $\alpha=2$.

Examples in Figures 12 and 13 facilitate the decision whether the samples belong to different tissues or not. The following examples, illustrated in Figures 14 and 15, will show that MFA can give us the decision whether the zoomed part of an image belongs to the particular image - parts of the same image have spectra similar to the spectrum of the whole image.

In Figure 14a the microscopy image called "cells" is depicted, while in Figure 14b only its zoomed part (under the white rectangle in Figure 14a) is shown. Corresponding spectra $f(\alpha)$, obtained by using FALFA, are depicted in Figure 14c. Now the maxima of both spectra are at the same location of α ($\alpha \approx 1.02$) although the

spectrum of the zoomed part is broader, indicating the higher variability of this signal.

This result is tested also by using the HISTMF routine. In Figure 15 the same medical image as in Figure 14 is shown, and two zoomed parts are investigated. All spectra, for the original image as well as for its magnified parts, have similar spectra with maxima at the same $\alpha=1.98$.

Note that spectra obtained by using different methods are not exactly the same (compare Figures 12c and 13, or 14c and 15) but the global shape is very close. The method (7) applied in the FALFA (a part of the MATPACK [9]) is derived from the Legendre spectrum, producing smooth curve line of $f(\alpha)$ (as the ideal parabola) but without fine details, which is observed by Levy Vehel, too (10). Conversely, the HISTMF packet (13), based on the histogram method (1), retains fine details but the spectrum is not smooth. Also, this method has a drawback; it is useless for negative (or alternate signed) signals (22).

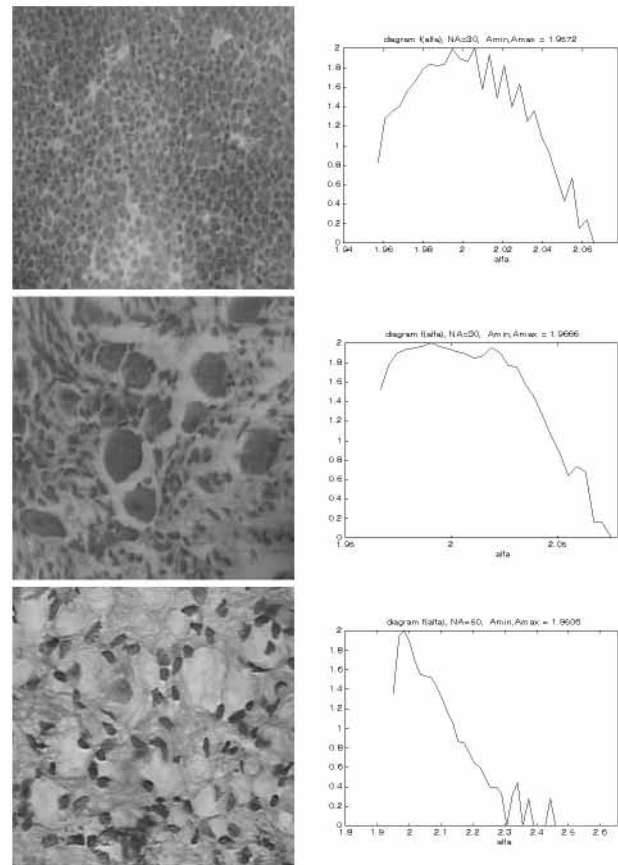


Figure 13. The MFA in sample classification - different samples

The idea of an inverse MF analysis (IMFA) for extracting characteristic details from an image is exposed first in (10). If we associate to each pixel the appropriate values of the parameter α and the spectrum $f(\alpha)$, a sort of inverse multifractal is obtained. Then, having in mind the local and the global behavior of quantities α and $f(\alpha)$, we can extract some particular image features without any image degradation. More precisely, points having α and $f(\alpha)$

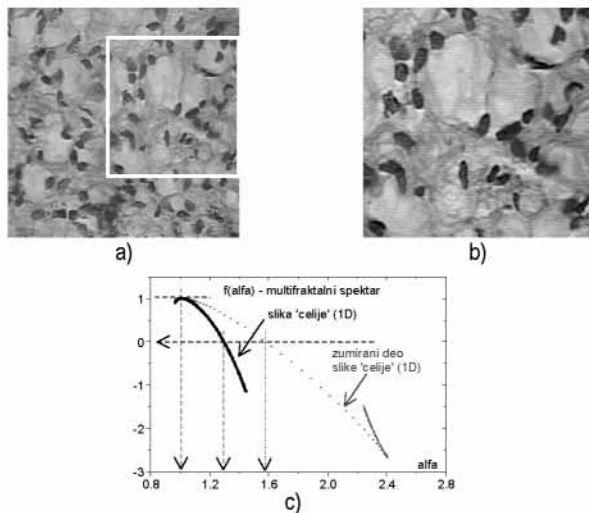


Figure 14. The MFA in sample classification: a) Original image and b) its zoomed part; c) Corresponding spectra

close to 1.0 corresponds to those belonging to the smooth line, i.e., they are the edge points, while points having α and $f(\alpha)$ close to 2.0 correspond to points on the flat surface. Any classic image processing method (in space or in transform domain) for region extracting is always followed by more or less image degradation (23,24). Digital images with 256 gray levels are processed in this way. Multifractal spectra are derived by using HISTMF routine (13). Several illustrative examples are depicted in Figures 16-17. In Figure 16 the IMFA is applied to the region extraction. The MRI brain image, Figure 16a, is under investigation (13). The series of images in Figure 16b-e contain image details characterized by different values of $f(\alpha)$: b) $f(\alpha) < 0.7$, c) $0.9 < f(\alpha) < 1.1$, d) $1.7 < f(\alpha) < 1.9$ and e) $f(\alpha) \cong 2.0$. Outputs are binary images: pixels having selected values of $f(\alpha)$ are remapped to level 1 (white) while the rest of the pixels are black. As we can see only the characteristic details are extracted without any image degradation - all details retain full sharpness and the unchangeable shapes.

The IMFA method seems to be a very promising tool in mammography (14). Namely, in mammography, it is very important to find calcification points into the tissue, as earlier as possible. An ordinary method uses the mammogram analysis (the X-ray images of the breast), but for better distinguishing fine details high X-ray doses are necessary. The IMFA can be an additional method in the mammogram analysis since in MF spectrum some (almost) invisible details can be extracted from the parts of the spectrum. This assertion is illustrated in Figure 17.

In Figure 17a a standard mammogram of dimension 1024x1024 pixels, with 4096 gray scale levels is depicted. From the whole image, its part of dimension 100x200 pixels is selected - under the white rectangle in Figure 17a - and for this part of image a MFA is performed. In Figure 17b the magnified selected part is depicted, while in Figure 17c its MF spectrum, obtained via

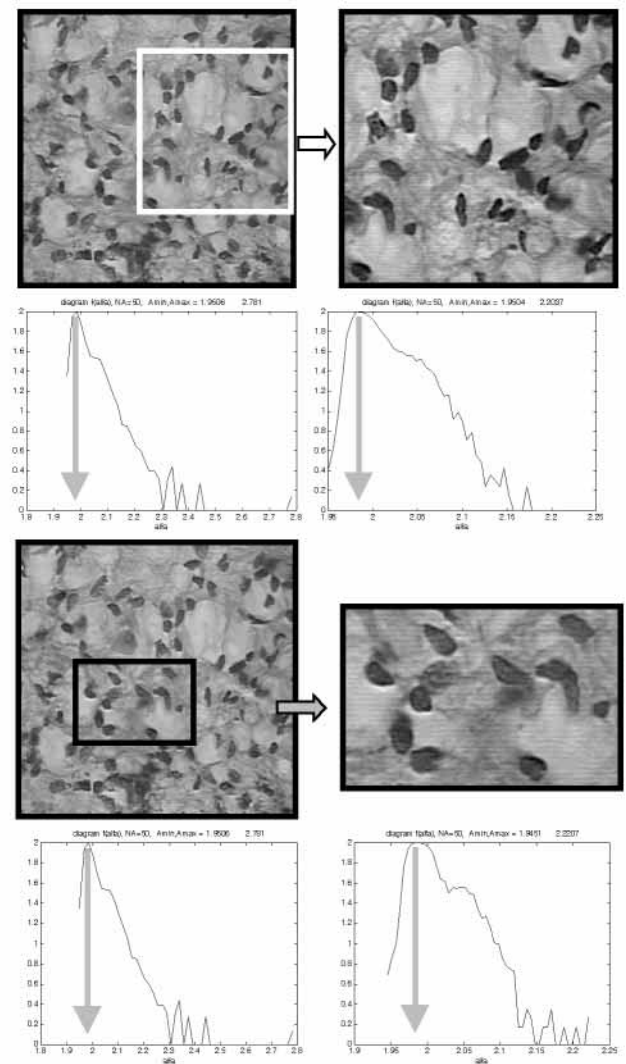


Figure 15. The MFA in sample classification: Original image (left) and its zoomed parts (right) and their corresponding spectra

HISTMF program (13), is plotted. From this image, sub-images containing pixels having particular values of the spectrum of $f(\alpha)$ - Figure 17d-f, or having particular values of parameter α - Figure 17g-i, are derived. Regions of $f(\alpha)$ and α are chosen arbitrarily. Extracted pixels are drawn as black ones while the background is gray.

CONCLUSION

The significance and the advantage of the fractal and multifractal analyses (FA and MFA) in signal processing, compared to "classic" signal processing lie in the way of how the non-regularities are assumed. The MFA tends to extract relevant information directly from the singularities. More precisely, based on the particular value of α and/or $f(\alpha)$, the non-homogenous points can be extracted from an original signal (10,13,14). By extracting image pixels having particular values of α or $f(\alpha)$, which can be called an inverse MFA (IMFA) we can extract particular image regions usually invisible. Moreover, this procedure does not provoke any

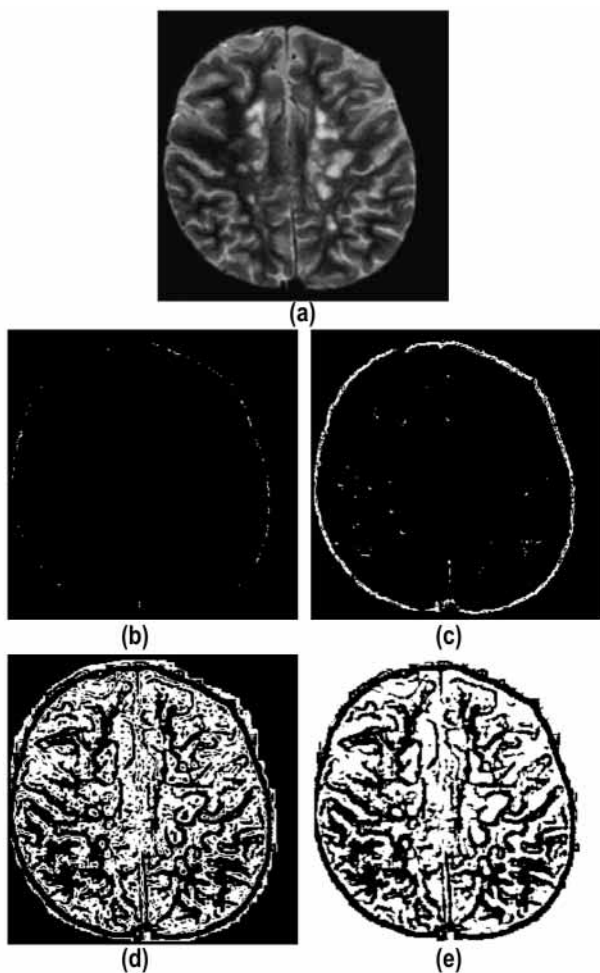


Figure 16. The IMFA in extracting characteristic image details: (a) An original MRI image, (b)-(e) MF images with: b) $f(\alpha) < 0.7$; c) $0.9 < f(\alpha) < 1.1$; d) $1.7 < f(\alpha) < 1.9$; e) $f(\alpha) \approx 2.0$

image degradation. This feature is very important for many applications, particularly in medical diagnosis. The IMFA application in medicine seems to be a very promising tool.

ACKNOWLEDGMENT

This work is partially supported by the Ministry of Science, Technology and Development, Republic of Serbia, under the Grant No. 2105.

REFERENCES

1. Peitgen H, Jurgens H, Saupe D. Chaos and Fractals. Berlin: Springer-Verlag; 1992.
2. Turner M, Blackledg J, Andrews P: Fractal Geometry in Digital Imaging. London : Academic Press, 1998.
3. Mandelbrot B , Les objets fractals: forme, hasard et dimension, 1975.
4. Uma K, Ramakrishnan KR, Ananthakrishna G. Image analysis using multifractals. Proceedings IEEE Conf. ICASSP-96. May 1996. Atlanta (USA)1996; 4:2188-2190.
5. Hausdorf F. Dimension und ausseres Mass. Math Ann 1919; 79: 157-179.

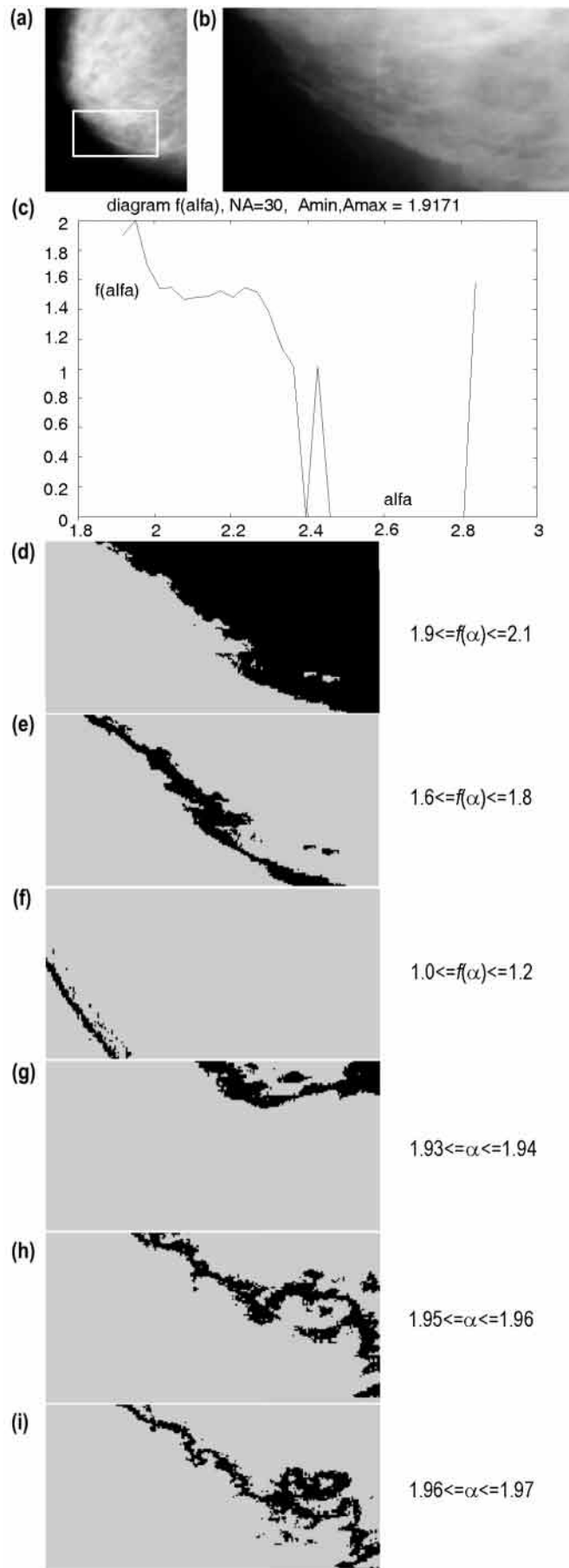


Figure 17. The IMFA applied in mammography

6. Falconer K. *Fractal Geometry, Mathematical Foundations and Applications*. Wiley; 1990.
7. Chhabra A, Jensen R. Direct determination of the $f(\alpha)$ singularity spectrum. *Phys Rev Lett*. 1989; 62:1327.
8. Gammel B. Multifractal. Sept.1996. http://www.physik.tu-muenchen.de/81/lehrstuehle/T32/matpack/html/matpack_frame.html.
9. Gammel B. Matpack Library Release 1.4. Jan 1999, <http://www.physik.tu-muenchen.de:81/.../Falpa/>
10. Vehel JL. Introduction to the multifractal analysis of image. 1996. <http://www-rocq.inria.fr/fractales>.
11. Bulmore W, Brammer M, Harvey I, Persaud R, Muray R, RonM . Fractal analysis of the boundary between the white matter and cerebral cortex in magnetic resonance images: A controlled study of schizophrenic and maniac-depressive patients. *Psychol Med*. 1994;24: 771-781.
12. Reljin I, Reljin B, Rakočević I, Mastorakis N. Image content described by fractal parameters. *Recent Advances in Signal Processing and Communications*. Mastorakis N (Ed.). Denvers: World Scientific Press; 1999:31-34.
13. Reljin I, Reljin B, Pavlović I, Rakočević I. Multifractal analysis of gray-scale images. *Proceedings IEEE 10th Mediterranean Electrotechnical Conference, MELECON-2000*. May 29-31. Lemesos, (Cyprus).2000;II:490-3.
14. Reljin B, Relji I. Multifractal medical image analysis and its possible application to mammograms. Philadelphia: Lecture notes in Thomas Jefferson University;2002.
15. Buldyrev S, Goldberger A, Havlin S, Peng C, Stanley H. Fractals in biology and medicine: From DNA to heartbeat. In Bunde A, Havlin S (Eds.). *Fractals in Science*. Berlin: Springer-Verlag;1994.p.49-87.
16. Cook M, Free S, Manfold M, Fish D, Shorvon S, Stevens J. Fractal description of cerebral cortical patterns in frontal lobe epilepsy. *Eur Neurol* 1995; 35: 327-335.
17. Cross S. Fractals in pathology. *J Pathol* 1997; 182:1-8.
18. Einstein A, Wu HS, Sanchez M, Gil J. Fractal characterization of chromatin appearance for diagnostic in breast cytology. *J Pathol* 1998;185: 366-381.
19. Sedivy R, Mader R. Fractals, chaos and cancer: Do they coincide?. *Cancer Invest* 1997; 15 (6): 601-607.
20. Budimilija Z. *Fractal Dimension of Neurons in Different Brain Regions After Cerebral Hypoxia* (dissertation). Belgrade: University of Belgrade; 2001.
21. Japundić-Žigon N. Contribution of computer supported methodology in determining the origin and the significance of the fast heart-rate variability.13 Yugoslav Congress of Cardiology. Novi Sad, Oct. 17-20. 2001.
22. Mandelbrot B. Negative fractal dimensions and multifractals. *Physica A* 1990; 163:306-15.
23. Jahne B. *Digital Image Processing: Concepts, Algorithms, and Scientific Applications*, Third. Ed. Berlin: Springer-Verlag; 1995.
24. Russ, *Image Processing Handbook*, Third ed. CRC Press; 2000.

FUSNOTE

¹ The Collier's Encyclopedia, London, 1986, states "The total mileage of the Britain coastline is slightly under 5,000 miles = 8,000 km, while the Encyclopedia Americana, New York, 1958, states "Britain has coasts totaling 4,650 miles = 7,440 km." (1)

² For instance, Theodor Weierstrass (1815-1897) created a continuous function that was nowhere differentiable; Felix Hausdorff (1869-1942) defined (and documented for many of 'pathological' functions) the non-integer dimension for point-sets which is a fraction greater than the corresponding topological dimension; Georg Cantor (1845-1918) created infinite point-set exhibiting fractal behavior (Cantor Set), Helge von Koch (1874-1924) and Waclaw Sierpinski (1882-1967) defined some rules for creating fractal objects (Koch curve i Sierpinski carpet), etc. (1,2).

NOTE

This papaer was presented on the 8th Academy of Studenica.